Geophysical Journal International

Geophys. J. Int. (2020) **222,** 544–559
Advance Access publication 2020 April 28
GJI Seismology

doi: 10.1093/gji/ggaa194

Retrieval of amplitude and attenuation from ambient seismic noise: synthetic data and practical considerations

Lianqing Zhou,[1] Xiaodong Song[2] and Richard L. Weaver[3]

[1] *Institute of Earthquake Forecasting, China Earthquake Administration, Beijing* 100036, *China*
[2] *Department of Geology, University of Illinois at Urbana-Champaign, Champaign,* IL61822, *USA. E-mail: xsong@illinois.edu*
[3] *Department of Physics, University of Illinois at Urbana-Champaign, Champaign,* IL61822, *USA*

Accepted 2020 April 15. Received 2020 April 5; in original form 2019 November 7

SUMMARY

Ambient noise correlation has been used extensively to retrieve traveltimes of surface waves. However, studies of retrieving amplitude information and attenuation from ambient noise are limited. In this study, we develop methods and strategies to extract Rayleigh wave amplitude and attenuation from ambient noise correlation, based on theoretical derivation, numerical simulation, and practical considerations of real seismic data. The synthetic data included a numerical simulation of a highly anisotropic noise source and Earth-like temporally varying strength. Results from synthetic data validate that amplitudes and attenuations can indeed be extracted from noise correlations for a linear array. A temporal flattening procedure is effective in speeding up convergence while preserving relative amplitudes. The traditional one-bit normalization and other types of temporal normalization that are applied to each individual station separately are problematic in recovering attenuation and should be avoided. In this study, we propose an 'asynchronous' temporal flattening procedure for real data that does not require all stations to have data at the same time. Furthermore, we present the detailed procedure for amplitude retrieval from ambient noise. Tests on real data suggest attenuations extracted from our noise-based methods are comparable with those from earthquakes. Our study shows an exciting promise of retrieving amplitude and attenuation information from ambient noise correlations and suggests practical considerations for applications to real data.

Key words: Computational seismology; Seismic attenuation; Seismic noise; Seismic tomography; Surface waves and free oscillations; Theoretical seismology.

1 INTRODUCTION

It has been demonstrated both in theory and by laboratory experiments that Green's functions (GFs) can be obtained from cross correlation (CC) of diffuse fields (Lobkis & Weaver 2001; Weaver 2001). This discovery was applied rapidly to seismology, especially in traveltime measurements of surface waves (e.g. Sabra *et al.* 2005; Shapiro *et al.* 2005; Kang & Shin 2006; Yao *et al.* 2006; Brenguier *et al.* 2007; Bensen *et al.* 2008; Lin *et al.* 2008; Yang *et al.* 2008b; Zheng *et al.* 2008). Elasticity and inelasticity are two important properties of Earth's media. The elastic wave speed is generally estimated by traveltimes of seismic waves; the inelastic property is generally characterized by attenuation of amplitudes of seismic waves. Compared to seismic velocity, seismic attenuation is a more critical parameter for reflecting temperature and fluid content in the Earth (Johnston *et al.* 1979; Toksöz 1979; Winkler & Nur 1979a, 1979b, 1982; Karato 1993, 2003; Priestley & McKenzie 2006; Adam *et al.* 2009; Zhou *et al.*2011a). Attenuation is also an important parameter for predicting ground motion from strong earthquakes, especially in sedimentary basins (e.g. Komatitsch *et al.* 2004; Olsen *et al.* 2006; Prieto *et al.* 2011; Zhou *et al.*2011b). Nevertheless, most studies have focused on measurements of traveltimes (or velocities) using empirical GFs from the Earth's ambient noise (for simplicity, we use the term GF hereafter whether it is a true GF or an approximation). Albeit by many fewer studies, it has also been shown possible to extract amplitude and attenuation information from ambient noise (Lobkis & Weaver 2001; Snieder & Safak 2006; Kohler *et al.* 2007; Larose *et al.* 2007; Matzel 2008; Prieto & Beroza 2008; Prieto *et al.* 2009; Taylor *et al.* 2009; Cupillard & Capdeville 2010; Froment *et al.* 2010; Cupillard *et al.* 2011; Lawrence & Prieto 2011; Lawrence *et al.* 2013; Lin *et al.* 2011; Prieto *et al.* 2011; Weaver 2011, 2013; Zhang & Yang 2013; Bowden *et al.* 2017; Stehly & Boué 2017).

A key issue in extracting the attenuation of Rayleigh waves from ambient noise is the nature of the ambient noise, which varies in time, strength, location and direction (Stehly *et al.* 2006; Gerstoft

& Tanimoto 2007; Yang *et al.* 2008a; Yao & Van Der Hilst 2009). Therefore, early experiments on extraction of surface wave amplitude from ambient noise to obtain attenuation are usually carried out based on relatively simple assumptions about the distribution of the noise sources. Based on a diffuse acoustic field, Lobkis & Weaver (2001) performed an experiment and recovered both phase and amplitude of waves from noise. Larose *et al.* (2007) used noise obtained from an air-jet forcing and observed that the retrieved amplitude decay from noise is consistent with the amplitude dependence expected from geometrical spreading and attenuation. Snieder & Safak (2006) and Kohler *et al.* (2007) showed that it is possible to retrieve attenuation information for buildings by deconvolution of seismic waves from an earthquake. Following a similar method, Prieto *et al.* (2010) used ambient vibrations to obtain the impulse response, which can be used to estimate attenuation values. Subsequently, both earthquake data (Nakata *et al.* 2013) and ambient vibrations (Nakata & Snieder 2014; Sun *et al.* 2017) were applied to monitor a building by deconvolution interferometry. Mordret *et al.* (2017) also used the method to estimate temporal changes of damping factors. Prieto & Beroza (2008) showed that relative amplitudes from ambient noise GFs obtained in this way coincided with those observed from nearby earthquakes. Using spectral coherency of the ambient field (Nakahara 2006), Prieto *et al.* (2009) claimed to recover both phase velocities and attenuation coefficients at different frequencies. Applications to southern California showed distinct differences in wave speeds and attenuation between paths traversing major basins and other paths. The method assumed that the ambient field is isotropic. Prieto *et al.* (2009) achieved this by azimuthal and regional averaging, and they claimed to obtain average attenuations for the regions of interest. But in Tsai's opinion (2011), for stations at large distances the coherency of noise is not a good approximation, and thus will introduce additional biases. Taylor *et al.* (2009) presented a methodology to obtain frequency-dependent relative site amplification factors by treating a seismic array as a forced damped harmonic oscillator system where each station responds to a forcing function obtained from frequency–wavenumber beams of the ambient noise field. Cupillard & Capdeville (2010) carried out numerical experiments and retrieved geometrical spreading as well as intrinsic attenuation in the case of a uniform distribution, even after strong non-linear operations such as one-bit normalization and spectral whitening were applied to the noise recordings. Tsai (2011) provided a ray-theoretical framework for quantifying amplitudes in noise correlation measurements and explicitly accounted for attenuation as well as the spatial distribution of sources. Using traditional ambient noise data processing procedures, Lin *et al.* (2011) asserted that common ambient noise data processing procedures such as temporal normalization and spectral whitening in amplitude retrieval can be retained as long as the amplitudes of the CCs are corrected appropriately, but the study is empirical and is not based on a theoretical framework. Using linear triplets of stations, Liu *et al.* (2015) extracted seismic attenuation coefficients from CCs of ambient noise. An improved inversion algorithm was developed to obtain amplitude and phase terms in the frequency domain. Taking advantage of a dense array such as the USArray, Bowden *et al.* (2017) proposed a wavefront tracking approach that utilizes ambient noise correlations to construct the entire wavefield and then to obtain site amplification and attenuation of Rayleigh waves across the USArray, taking into consideration focusing and defocusing effects of the wave propagation. They used a modified spectral whitening approach that weights the spectra of all stations by a single spectrum to preserve the relative amplitudes between stations (Bowden *et al.* 2015). This method can eliminate the influence of the noise source distribution to a certain extent by constructing the whole wave field, but it needs dense two-dimensional arrays and accurate deduction of propagation effect.

Another key issue in extracting the attenuation of surface waves from ambient noise is using an appropriate pre-processing procedure. One-bit normalization, which clips all amplitude information, is a typical pre-processing procedure to extract amplitudes of GFs from ambient noise (Larose *et al.* 2007; Matzel 2007; Cupillard & Capdeville 2010; Cupillard *et al.* 2011; Groos *et al.* 2011; Lin *et al.* 2011; Weaver 2011). However, whether one-bit normalization is sufficient to retrieve accurate amplitudes of GFs from ambient noise is not clear. Matzel (2007) showed that one-bit signals may preserve amplitude information. Using numerical simulation, Cupillard & Capdeville (2010) and Cupillard *et al.* (2011) found that both in the case of a uniform distribution and a non-uniform distribution of sources, intrinsic attenuation is retrieved even after strong non-linear operations such as one-bit normalization are applied to the ambient noise data. Lin *et al*. (2011) demonstrated that common processing procedures on ambient noise data can be retained as long as the amplitudes of the CCs are corrected for the duration time of noise, geometrical spreading, and the azimuthal variation in the strength of ambient noise sources. However, Larose *et al.* (2007) suggested that although one-bit pre-processing is helpful to reconstruct the phase of the GF, it should not be used to reconstruct the amplitude of the surface wave. Using a numerical simulation, Weaver (2011) proved theoretically that, in the case of smoothly varying noise sources, one-bit pre-processing would distort the apparent attenuation of GFs. Viens *et al.* (2017) computed impulse response functions using CC, coherency and deconvolution techniques of the raw ambient seismic field and the CC of one-bit normalized data. They compared the amplitudes to a real earthquake, indicating that the one-bit normalization method is not a good choice to retrieve amplitudes of ambient noise.

In general, most of the above-mentioned methods used in extracting surface wave amplitudes are empirical with strict requirements on the properties of ambient noise. However, complex natural ambient noise cannot easily satisfy such strict requirements. As a result, there is much debate on these different processing methods. From theoretical derivations and numerical simulations, Weaver (2011) suggests that from the ray arrival amplitudes, the ambient field's specific intensity, the strength and, most importantly, attenuation can be recovered, even for incompletely diffuse noise fields.

This study is an attempt to develop methods and strategies to extract attenuation for the real Earth from ambient noise correlation. Our approach is based on the theory of Weaver (2011), but considers complications from the natural ambient noise and seismic vibrations of the Earth. We use ambient noise data synthetized by simulated noise generated from anisotropic sources and natural seismic noise recorded by USArray. We also use earthquake records to test the methodologies. We demonstrate that the relative amplitudes between station pairs and thus the medium attenuation can indeed be retrieved from ambient noise correlation after careful processing procedures. Below, we first outline our basic methodology, following Weaver (2011). We then use synthetic data to show that amplitude and attenuation can be recovered from noise correlation after applying a key 'temporal flattening' (TF) data processing procedure (Weaver 2011). Next we deal with real seismic data, where we propose a modified data processing procedure called 'asynchronous' temporal flattening (ATF). We show the feasibility of attenuation retrieval from real

data examples by comparing the attenuation results retrieved from seismic ambient noise with those retrieved from earthquakes. We specify steps by which amplitudes can be retrieved from ambient noise, and perform a series of tests for parameter selections in data processing.

2 METHODS

Our basic approach relies on a recent theoretical derivation by Weaver (2011, 2013) in the case of an incompletely diffuse noise field. A fully diffuse wave field is usually defined as one that is globally equipartitioned. It has all normal modes excited with uncorrelated amplitudes and the disturbance is an isotropic random superposition of plane waves at each point of the vibrating medium at a given frequency (Weaver 1982; Lobkis & Weaver 2001). However, because long-period seismic noise fields are directional (Weaver 2011), the natural seismic noise field is often not a fully diffused noise field. Weaver (2011, 2013)'s studies show that even in the case of an incompletely diffuse noise field, the amplitude of the GF from the CC between two stations can be expressed explicitly as a function of the wave attenuation α and the intensity of the diffuse wave field B. If the noise intensity changes smoothly in space and direction, the amplitude X of a Rayleigh wave cross-correlation function between stations i and j shows that it takes the form, to the first order

$$X_{ij} = 2s_i s_j B_i(\hat{\mathbf{n}}_{i\to j})\sqrt{2\pi c/(\omega_o|x_i - x_j|)}\ \exp(-\alpha|x_i - x_j|), \tag{1}$$

where α is the average attenuation between stations i and j; ω_o is the frequency; $\sqrt{2\pi c/(\omega_o|x_i - x_j|)}$ is the geometrical spreading term; c is wave speed and s_i and s_j are site effects at the two stations. B_i is the ambient intensity in the direction from i towards j evaluated at station i. An important and useful result for the research reported here is that the ray amplitude X depends only on B in that direction as an asymptotically valid approximation (at the next order, the differences with respect to direction are of order 1 per cent or less) (Weaver 2011).

The surprisingly simple result (eq. 1) makes it relatively easy to retrieve attenuation along a linear array. For a linear array, along a direction $\hat{\mathbf{n}}$ of several seismic stations, the amplitudes X_{ij} of CC arrivals for $j > i$ should be

$$X_{i<j} = 2s_i s_j B_i(\hat{\mathbf{n}}_{i\to j})\sqrt{2\pi c/(\omega_o|x_i - x_j|)}\ \exp\left(-\int_{x_i}^{x_j}\alpha \mathrm{d}x\right). \tag{2}$$

Eq. (2) indicates that amplitude X from station i (near one end of the array) to all stations j in one direction (to the other end of the array) depends only on the intensity at station i along the same direction. Thus, for a linear array, we can formulate the following strategies to retrieve attenuation.

From eq. (2), we can obtain an estimate of the path-averaged attenuation easily. Consider a set of linearly arranged stations S_1, S_2, S_3 and S_1 is the reference station. The amplitude of the GF from S_1 to S_2, $X_{1\to2}$, and that of the GF from S_1 to S_3, $X_{1\to3}$ are as denoted by

$$X_{1\to2} = 2s_1 s_2 B_1(\hat{\mathbf{n}}_{1\to2})\sqrt{2\pi c/\omega\,|x_1 - x_2|}\exp\left(-\int_{\vec{r}_1}^{\vec{r}_2}\alpha_{12}\mathrm{d}x\right), \tag{3}$$

$$X_{1\to3} = 2s_1 s_3 B_1(\hat{\mathbf{n}}_{1\to3})\sqrt{2\pi c/\omega\,|x_1 - x_3|}\exp\left(-\int_{\vec{r}_1}^{\vec{r}_3}\alpha_{13}\mathrm{d}x\right), \tag{4}$$

where α_{12} is the attenuation coefficient of the medium between S_1 and S_2, and α_{13} is that between S_1 and S_3. The surface wave amplitude ratio of the two stations is

$$\frac{X_{1\to3}}{X_{1\to2}} = \frac{\sqrt{|x_1 - x_3|}}{\sqrt{|x_1 - x_2|}}\frac{s_3}{s_2}\exp\left((-\int_{\vec{r}_2}^{\vec{r}_3}\alpha_{23}\mathrm{d}x\right). \tag{5}$$

Since the intensity of the noise sources at S_1 towards S_2 and S_3 are equal, the logarithm on both sides of the above formula can be expressed as

$$\ln\frac{X_{1\to3}}{X_{1\to2}} = \ln\frac{\sqrt{|x_1 - x_3|}}{\sqrt{|x_1 - x_2|}} + \ln s_3 - \ln s_2 - \alpha_{23}(x_3 - x_2). \tag{6}$$

With the above equation, we can invert the average attenuation factor of the medium between S_2 and S_3, α_{23}, and the site response of the stations S_2 and S_3 simultaneously. In this study, we set the site responses of all stations to 1, so the attenuation coefficient α_{23} of the medium between the two stations S_2 and S_3 can be directly solved.

In the real Earth, linear deployments are common, thus the above approaches can be applied. However, more commonly, we have a network of stations in 2-D. In such a case, we can form a series of linear arrays, much like the classical 2-station method of the earthquake-based surface wave tomography of wave speeds (e.g.; Yao *et al.* 2006). A similar idea has also been applied to traditional earthquake-based attenuation studies (e.g. Yang *et al.* 2004). In this study, we focused only on the path-averaged attenuation and did not consider site factors in the derivation of average attenuation values.

3 AMPLITUDE AND ATTENUATION RETRIEVAL FROM SYNTHETIC DATA

3.1 Synthetic noise wavefield

3.1.1 Original simulated noise data

Based on a discrete 271 × 271 mesh representing a square two-dimensional domain, we simulated a noise field for an anisotropic noise source distribution (Fig. 1). The source intensity included a smoothly varying component and a strong 'local' intensity (as indicated from the shade on the source 'ring'). The study region contained two quadrants, inside the source 'ring'. Details of the scheme for the numerical simulation can be found in Weaver (2013). The numbers below are scaled to seismic observations, for easier understanding. Without loss of generality, we focus on waves with a narrow band pass filter in the vicinity of the period of 10 s in the numerical tests. A linear array of 10 receiver stations with spacing distance of 85 km was placed diagonally across two quadrants inside the ring, where 5 receiver stations are in the lower-left quadrant and the other 5 receiver stations are located in the upper-right quadrant. The wave speed is set at 3 km/s. An attenuation model was configured with two different attenuation coefficients, $\alpha_1 = 0.00259$ km^{-1} in the lower-left quadrant (quadrant 1) and $\alpha_2 = 0.00388$ km^{-1} in the upper-right quadrant (quadrant 2), which correspond to attenuation factor Q of 40.4 and 27.0, respectively. The low Q values were

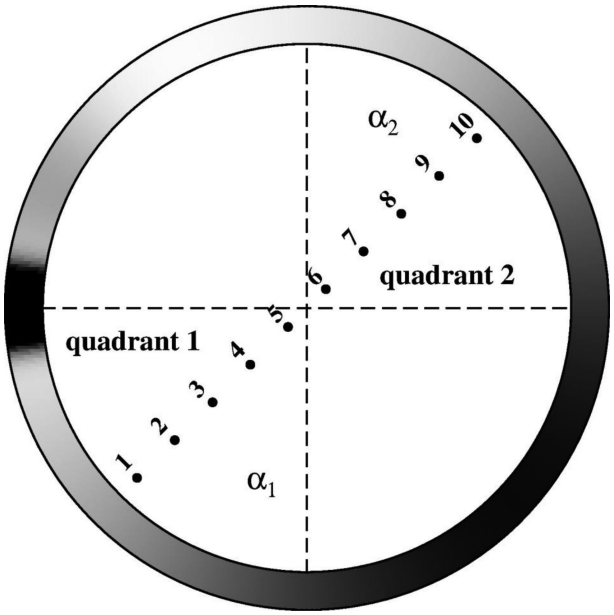

Figure 1. Set up of numerical simulation, showing distribution of source intensity and receiver locations. The distribution of the Gaussian noise source is highly non-uniform as indicated by the shades along the circumference (higher intensity in darker shade). The input attenuation coefficients are $\alpha_1 = 0.00259$ km^{-1} and $\alpha_2 = 0.00388$ km^{-1}, for lower-left quadrant (quadrant 1) and upper-right quadrant (quadrant 2), respectively.

chosen so that the attenuation effect on amplitudes can be clearly visible. The site responses of all stations in the experiment were set to 1. There is no internal scattering. The sample rate of the data is 3 points per second, and a total of about 1 yr of data was generated at each station.

3.1.2 Synthetic seismic noise data with temporally varying strength

We multiplied our simulated noise data by the absolute value of the recorded seismic noise from an actual station our simulated noise data to obtain synthetic data with temporally variable amplitude similar to natural seismic noise. The seismic noise was from a 9-yr continuous seismic waveform of a station in Southern California (station Isabella) at 1 sample per second. The station selection was somewhat arbitrary, but the long continuous record of the station does provide a real representation of the variation of the Earth's ambient noise strength. The original simulated data consisted of a series of file segments of about 63 000 points (or a little less than 6 hr of data at 3 samples per second) per segment. On the other hand, the seismic data were divided into a series of 1-d file segments (or 86 400 data points at 1 sample per second). For each segment, we then multiplied the absolute value of the seismic trace with the simulated noise trace point by point, to generate a new synthetic noise field with temporally varying strength (Fig. 2). The rest of the unused data points in the seismic trace were discarded. Note that the seismic trace and the simulated noise field have different sampling rates, but the difference does not matter as we are only interested in generating a noise field with temporally varying strength as in the real Earth. Note also that the absolute value of the same seismic trace is multiplied the simulated noise field at all the stations; the temporal variation of the noise strength is thus similar at all the stations. Thus, the simulated data are not the same as real data, which have different noise strength and earthquake arrival times and amplitudes.

The purpose is to introduce varying noise strength into the simulation in order to examine the convergence rate of the GFs and the relative amplitudes between the GFs. We will examine situations with real data later, which require a modification of data processing procedure (Section 4). In our discussion below, we refer to the original simulation data as 'original' and the data with seismic noise as 'raw' (Fig. 2). We did not remove earthquake or other energetic sources in the seismic trace so that the variation of strength of the 'raw' noise data is more Earth-like.

The reasons that we used the same seismic trace (rather than different seismic traces) to combine with the 'original' simulated noise traces to create the 'raw' traces are as follows. (1) Our purpose of creating the 'raw' data is to test different pre-processing techniques (see below) on the fidelity of the GF amplitudes and the convergence rate when the noise strength varies with time. The coherent noise that gives rise to the GFs comes from the 'original' traces, not from the strength variation. The created 'raw' traces are essentially the same as the traces generated with the same source spatial distribution as in Fig. 1 but with the temporal strength that varies as the imposed trace. In the real Earth, the temporal change of the noise strength is generally much slower than the propagation of the Rayleigh waves. Thus imposing the same temporally variable strength to all the stations in the array can provide a reasonable representation of the strength variation in the real Earth. (2) An alternative may be to use different seismic traces (e.g. from an array of real seismic stations) for the same time duration to impose the strength variation on the simulation stations. We would need to find stations with long recording history with few data gaps. The 'raw' data created as such may produce arrivals of wave propagation from earthquakes or earth's own ambient noise in the correlations, which may unnecessarily cause confusion with the correlated arrivals from the 'original' simulated noise.

3.2 Pre-processing: temporal flattening (TF) technique

Because seismic records contain energetic sources (e.g. earthquakes) and noise sources of varying strengths, pre-processing is needed in order to speed up the convergence from the CC to the GF and to increase the signal-to-noise ratio (SNR). One-bit (sign-bit) normalization is commonly used as a pre-processing technique to extract traveltimes of the seismic surface waves between two receivers in studies of seismic noise interferometry (e.g. Campillo & Paul 2003; Shapiro & Campillo 2004; Shapiro *et al.* 2005; Yao *et al.* 2006; Bensen *et al.* 2007).

In previous studies, one-bit normalization or other types of temporal normalization are applied to each individual station separately. To preserve the amplitudes of the GF, Weaver (2011) proposed a TF method, in which every station's band-limited signal is normalized by a running average of the total band-limited energy of all the stations. Thus each station is treated equally so that relative amplitudes are preserved (Bowden *et al.* 2015, 2017). In this study, we performed the TF normalization as follows. Each 1-d continuous record is divided into 2-hr segments. For each segment, the TF normalization factor is obtained by calculating the RMS of all the points of all the traces within the 2-hr segment. For that segment, each trace is divided by the TF normalization factor (the same global factor for all the traces).

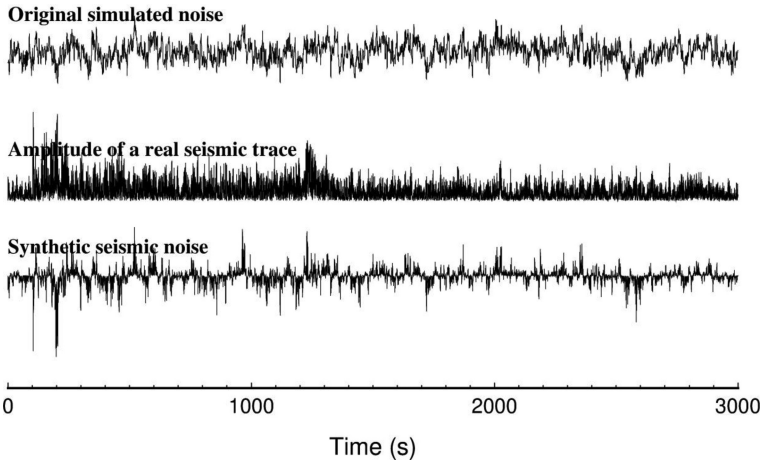

Figure 2. Synthetic noise data. Plotted are only a small segment (50 min) of data used in this study. (a) Original noise data from numerical simulation (Fig. 1). (b) Absolute amplitude of a real seismogram. The segment contains energy from an earthquake. (c) Synthetic seismic noise data. The trace was obtained by multiplying the original simulated trace (a) with the amplitude trace of the seismic noise data (b).

3.3 Results from simulated data

3.3.1 Comparison of different pre-processing techniques

We now apply different temporal normalization methods (one-bit, TF or no temporal normalization) to the 'original' and 'raw' synthetic data. The data processing procedure is as follows: (1) apply a cosine-bell shaped filter centred on 10 s with a 8 to 12-s band, (2) apply temporal normalization and (3) perform CC processing.

The GFs obtained from original and raw data without any normalization are shown as Figs 3(a) and (b), respectively, and those obtained from raw data with one-bit and TF normalization are shown as Figs 3(c) and (d), respectively. To compare the amplitude attenuation, we show the GFs of station pairs originating in a common station (e.g. station 1 'S01' in Fig. 3, the positive delay time lags). The amplitude of the GF originating in station 1 clearly decays as the interstation distance increases, which is expected from the geometrical spreading and attenuation (Weaver 2011; eq. 1).

Note that the GFs are highly asymmetric. The amplitude of the negative lag (from quadrant 2 to quadrant 1) is much smaller. This is because α_2 is much larger than α_1 and intensity deceases as $e^{-2\alpha|x_i-x_j|}$ (Weaver 2011). In addition, the intensity originating in station 1 in the direction to station 10 is more than 30 per cent greater than that originating in station 10 in the direction to station 1. Note also the strong energy at zero time in Figs 3(b)–(d), which is an autocorrelation artefact because the same temporally varying noise strength was embedded in the raw data of all the stations (see above).

From Fig. 3, we can clearly detect that GFs from original, one-bit, and TF processing data have good convergence, shown as waveforms with high SNR in the CC waveforms, while the GFs obtained from the raw data without any normalization have low SNR, especially when the spacing distances of station pairs is large. This result is consistent to that we expected, because the same problem also exists in the study of extracting surface wave velocity from ambient noise (Bensen *et al.* 2007). These temporal normalization methods effectively accelerate the convergence of the cross-correlation function and thus improve the SNR. Without the pre-processing of temporal normalization, several months of seismic ambient noise records may be dominated by the energy of a few earthquakes, and the GFs represents the correlation of signals from a few point sources rather than the correlation of the whole diffuse wavefield. We compare the GFs of two station pairs of S01–S03 and S01–S07 extracted from the three kinds of pre-processing data (raw: no temporal normalization used; one-bit: one-bit normalization used; flattening (TF): temporal flattening used) to determine whether the amplitude of the GFs are retrieved correctly. After the maximum amplitudes of GFs of the station pair S01–S03 obtained from different data are set to 1, the relative amplitudes of the station pair S01–S07 to those of S01–S03 obtained from raw and TF data are in agreement although the SNR from the raw data is quite low, and we also note that the relative amplitudes from one-bit data are not consistent with those from the other two processing methods (Fig. 4) (see more discussion below).

3.3.2 Attenuation retrieval

Fig. 5 compares relative amplitudes of the GFs extracted from different noise data and different temporal normalization methods. We show two cases: the case of station pairs originating in station 1 (Fig. 5a) and the case of station pairs originating in station 10 (Fig. 5b). Amplitude from station 1 to station 2 is greater than that from station 10 to station 9 (by 1.36), because of the anisotropic noise intensity distribution (Fig. 1). We can make the following conclusions from Fig. 5.

(1) The amplitude decay using the 'original' noise data agrees in the attenuation factors with the input model. This is not surprising and has been demonstrated by Weaver (2011) in theory and in numerical simulations.

(2) The amplitudes from one-bit normalization differ significantly from true values. They do not behave linearly. The amplitudes decay sometimes faster and sometime slower than those from real attenuation. Thus, one-bit normalization should be avoided in amplitude and attenuation extraction (Weaver 2013).

(3) The results from the 'raw' data (without any normalization) vary. When the amplitudes are large with good SNR of the GFs, the results agree with those from the 'original' (without any normalization). However, when SNR decreases (the amplitudes are small), the results from the 'raw' data can be significantly different from the true values as shown in the lower half of Fig. 5(b). In this case, the GFs from the 'raw' data have not converged because no normalization has been applied.

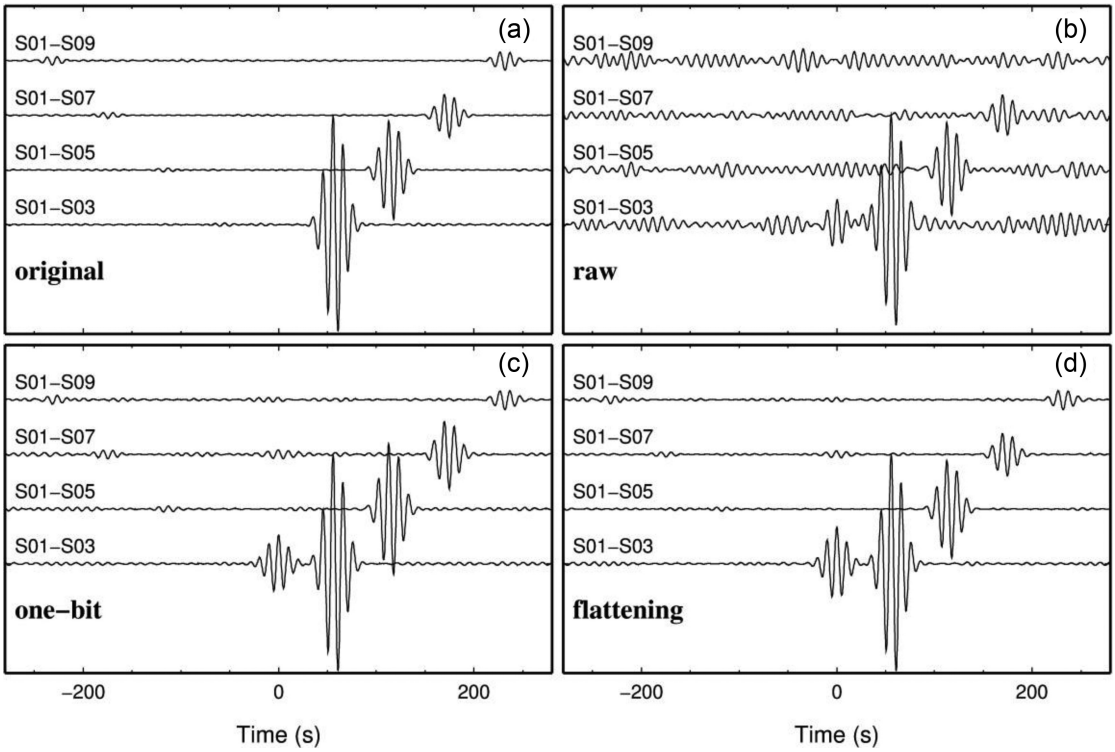

Figure 3. Green's functions obtained from synthetic noise data. The right-going GFs of the station pairs (e.g. S01–S03 means from S01 to S03) are at the positive time lag, which are generated by the common noise source strength at station 1. The left-going GFs (very weak) are at the negative time lag, which are generated by noise source strength at different stations (e.g. from S03 to S01). (a) GFs obtained from cross-correlations (CCs) of the original simulated noise data. (b–d) GFs obtained from CCs of the synthetic seismic noise data using different pre-processing procedures, respectively, that is (b) no pre-processing (raw), (c) one-bit and (d) temporal flattening (TF).

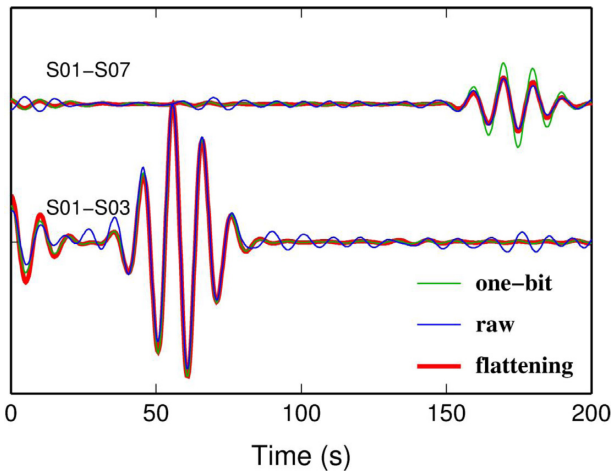

Figure 4. Comparison of amplitudes of GFs of two station pairs (labeled) obtained from synthetic seismic noise data with different pre-processing procedures (raw, thin blue; one-bit, thin green and TF, thick red).

(4) The relative amplitudes using the 'raw' data and TF normalization are similar to those from the 'original' data. Thus, the relative amplitude information can be retrieved from the TF pre-processing and the attenuation can be recovered. Essentially, the TF pre-processing speeds up the convergence because it reduces the influence of variable noise strength to make the noise field more diffuse. But it also preserves the relative amplitudes between different pairs because the same global normalization factor is applied to all the stations for the same time segment.

In summary, correlations using the raw data preserve the relative amplitudes of the GFs, but the convergence is too slow. The one-bit normalization speeds up the convergence but results in wrong amplitudes. The TF normalization achieves both.

4 AMPLITUDE RETRIEVAL FROM REAL DATA

As we have shown with synthetic data, amplitude information and attenuation can be extracted from a noise field, even when the spatial distribution of the noise source is highly anisotropic (as in Fig. 1) and the temporal source strength variation is Earth-like (such as the 'raw' data). The TF normalization is effective in speeding up the convergence of the GF while preserving amplitude information for the retrieval of attenuation. In the next section, we examine real seismic data, including the feasibility of amplitude and attenuation retrieval, data processing strategies, stability and convergence of GF amplitudes and comparison of attenuations from the ambient noise CCs and from earthquakes.

4.1 Seismic data

We selected four broad-band stations of the U.S. Reference Network (RN) (US.BOZ, CI.PASC, IU.RSSD and TA.KSCO) in western continental U.S. for testing data processing procedures and parameters (Fig. 6). Four years of continuous waveforms from 1st January 2008 to 31st December 2012 were used to construct the GFs. Data from 47 broad-band stations of the U.S. backbone network in the western continental U.S. were used to

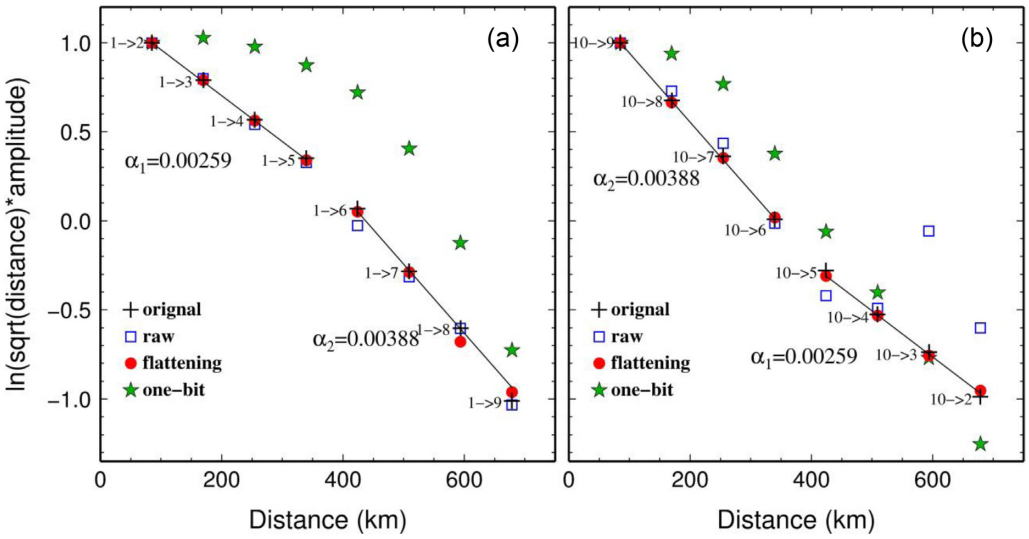

Figure 5. Relative amplitudes (symbols) extracted from GFs with different temporal normalization methods using synthetic data for two cases: station pairs originating at station 1 (a) and station pairs originating at station 10 (b). Plotted is the natural logarithm of the amplitude ratio corrected for geometrical spreading (square root of interstation distance). Because different temporal normalizations yield different absolute amplitudes, the amplitudes have been shifted so that the largest logarithm value is at 1. The amplitude of station pair 1 to 2 is about 1.36 times that of station pair 10 to 9. The slopes indicated by the solid lines are the true values of the attenuation factors from the input model.

check the convergence speed of the amplitudes of the GFs. For most stations the data are from more than 4 yr of successive recordings.

Finally, to demonstrate the feasibility of attenuation retrieval from ambient noise by comparing the results with those extracted from two earthquakes recorded by the same stations, we selected two groups of stations along two lines, including 121 stations in the west and 115 stations in the east.

4.2 Data processing and asynchronous temporal flattening (ATF) normalization method

The basic data processing procedure is very similar to that of numerous studies to obtain GFs to extract traveltimes from ambient noise correlations (e.g. Bensen *et al.* 2007), which generally involves data pre-processing (instrument response removal, time-domain normalization, broad band-pass filtering, and spectral whitening), CC on each day's seismograms between stations, stacking of all the correlations to get the GFs, and quality control on the GFs (e.g. Sun *et al.* 2010). However, there are three key differences in this study. First, data pre-processing is performed on all the stations simultaneously (TF pre-processing), whereas it has been done separately on each trace in previous studies. Secondly, we introduce the so-called asynchronous temporal flattening (ATF) temporal normalization method, in order to extract the amplitude information and to take into account practical problems of the actual seismic data. Thirdly, a narrow bandpass (rather than broad band-pass) filter is applied before the CC. This means that the spectral whitening commonly used in traveltime extraction from ambient noise, is not needed. The steps to extract amplitudes from ambient noise correlation are as follows (Fig. 7):

(1) Waveform data are prepared for each station individually, which we call our 'raw data'. Raw data are cut into a sequence of 1-d units, and then each station's instrument response is removed. This step is necessary for any amplitude-related studies because the amplification and frequency response of instruments in each stations may not be the same, affecting the observed amplitudes.

(2) The raw continuous waveforms are filtered by a narrow-band filter at each period of interest. The narrow-band filter is a cosine-bell-shaped filter centred on 10 s with an 8 to 12-s band, or 20 s with an 18 to 22-s band, respectively, for the 10-s or 20-s Rayleigh wave in this study.

(3) Energetic amplitudes are muted from the waveforms. Generally, the energy of earthquakes and spikes in continuous waveforms is much stronger than that of the ambient noise (Fig. 8). Furthermore, they generally appear in different time windows across a network of stations. If the earthquakes and spikes are not removed appropriately, amplitudes of CCs will be dominated by earthquakes and spikes, which will distort attenuation measurements. The energetic amplitudes are muted as follows (Fig. 8). For each moving data point, the amplitude at that point is divided by the RMS amplitude of the following 20-min time window. If the ratio is greater than 10, the amplitudes of that point and all the points in the following 20 min are set to zero.

(4) ATF normalization. The TF procedure we described above for the synthetic data is a synchronous operation, thus we call it 'synchronous temporal flattening (STF)'. To apply the STF for each time window, all the stations must have data for the entire window. Furthermore, because energetic amplitudes (earthquakes or spikes) generally appear at different time windows across the array of stations, if energetic signals are detected in one station, all the stations need to be muted for that time window. This operation is too restrictive for real Earth, leaving very small amount of usable data. We propose an alternative procedure, which we call 'asynchronous temporal flattening (ATF)'.

The ATF normalization procedure is as follows. First, energetic amplitudes in each station are removed separately using the procedure described above in step 3. Secondly, the energetic amplitudes are muted and only their positions are retained, as a result that the energetic track is kept of the removed amplitudes. Because earthquakes

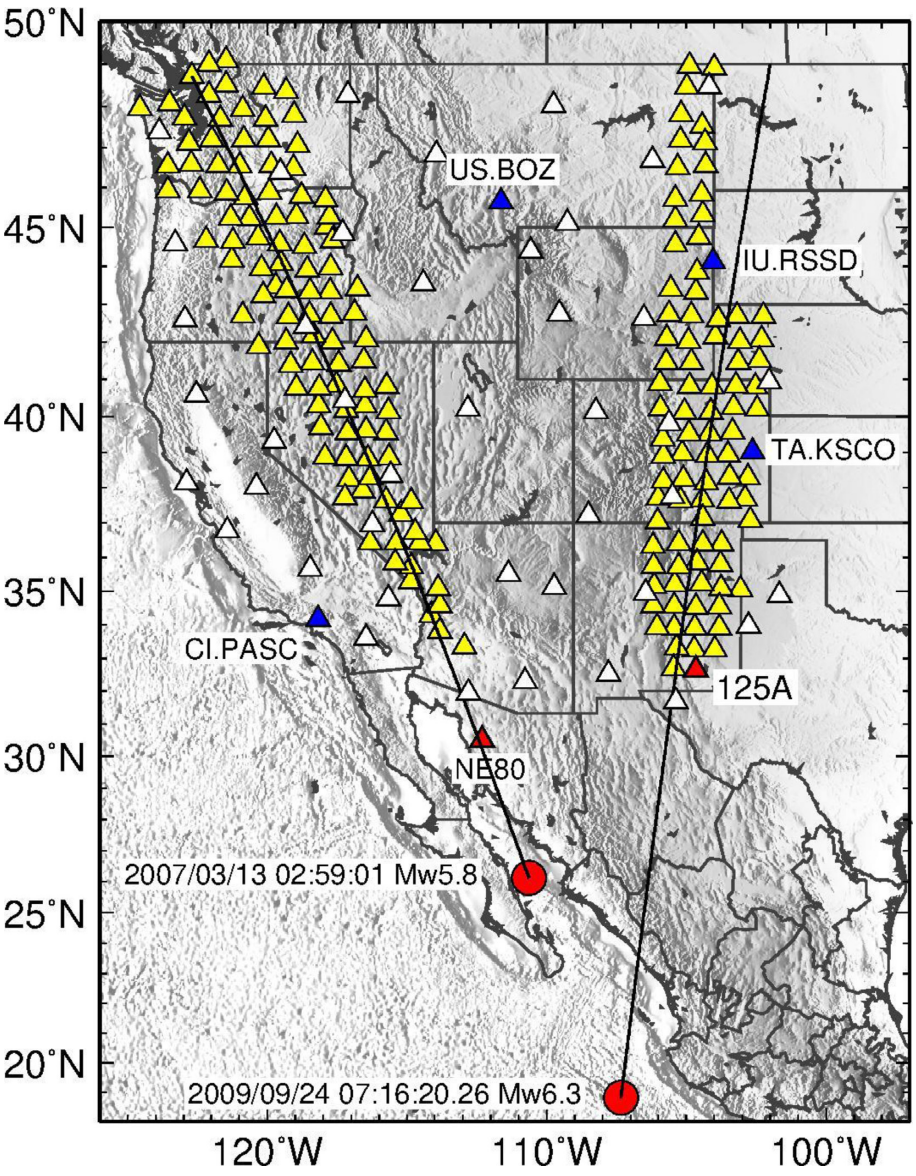

Figure 6. Distribution of seismic stations (triangles) in western U.S. and two earthquakes used in this study. There are three groups of stations: four U.S. Reference Network stations used to test data processing procedures (blue triangles); 47 stations of the U.S. backbone network used to examine the convergence of the amplitudes of the GFs (white triangles); and two nearly linear arrays used to compare attenuation factors retrieved from the two earthquakes and ambient noise correlations. The arrays have 121 and 115 stations, in the West Line and the East Line. Stations NE80 and 125A (red triangles) are the reference stations for the West Line and the East Line, respectively. The two earthquakes on 13 March 2007 (M_w 5.8) and 24 September 2009 (M_w 6.3) are used for the West Line and East Line, respectively.

or spikes exist in different time domains, a flag waveform is constructed for each station, which contains 1 or 0 at each sampling point for an effective (i.e. the original) point or a removed amplitude, respectively. When there is no data available or amplitudes are muted in the trace, the amplitudes of the corresponding positions in the flag waveform are set to 0. Otherwise, the amplitudes of the corresponding positions are set to 1. Thirdly, each day's data are divided into several segments of a selected length (e.g. 2 hr). Only stations with nonzero data in the flag waveforms are used. The RMS amplitude of all the nonzero data points in the flag waveforms in each time window is calculated. And then, each data point at each station in that time window is divided by the RMS amplitude above to obtain the normalized waveforms. Because the same global normalization factor is used for each time window, the relative amplitudes between different stations and hence those between the station-station CCs are preserved.

(5) Corrections on the GF amplitudes (Fig. 9). Because data at different stations are muted at different times, the numbers of effective data points contributing to the station–station CCs may be different for different station pairs and at different lag times. Thus the GF amplitudes need to be corrected. A simple way is to use the CC of the flag traces. The CC of the flag traces are defined by $C(n) = \frac{1}{N}\sum_{i=0}^{N-1} f_1(m)f_2(m+n)$, where $f_1(m)$ and $f_2(m)$ are the two flag traces of the corresponding signal and $C(n)$ is the CC of the two flag traces, and N is the effective point number of the flag traces used to

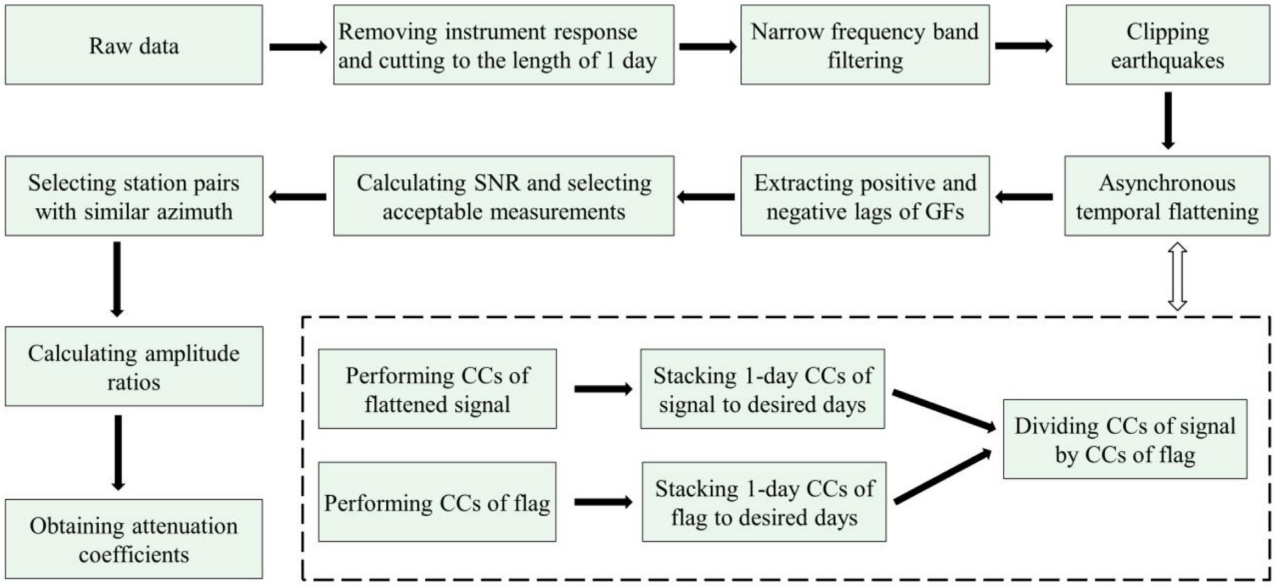

Figure 7. Flow chart for extracting amplitudes and attenuation with a linear array from ambient noise.

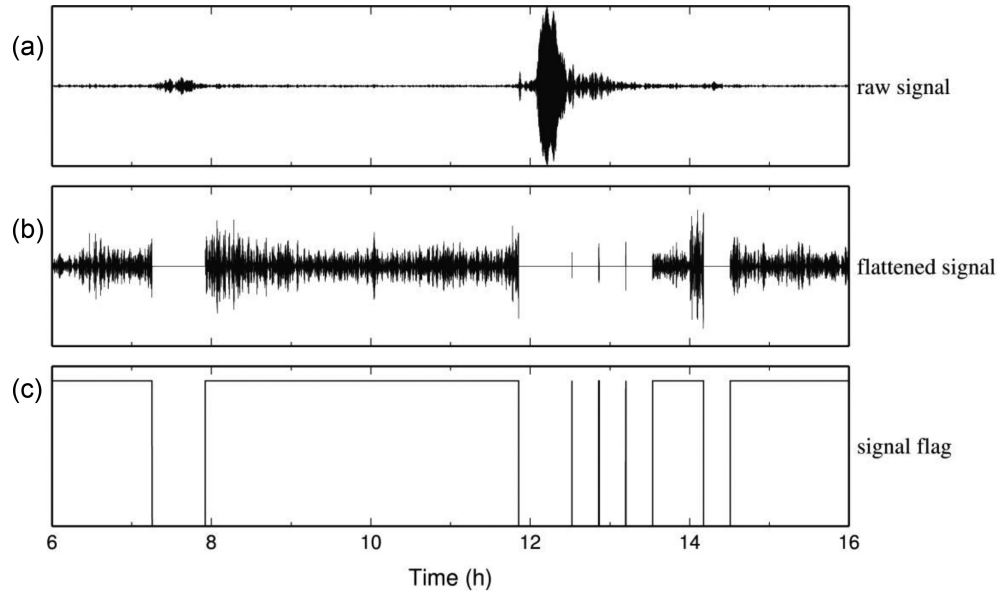

Figure 8. A generic example showing data processing procedure of asynchronous temporal flattening (ATF). (a) A raw continuous seismogram with the presence of earthquakes. (b) The new 'flattened' trace after earthquake muting (0 amplitude) and ATF. (c) The flag trace accompanying the flattened trace containing value of either 1 (no muting) or 0 (with muting).

conduct CC. The CC of flag procedure is as follows. CC of each 1-d of the normalized waveforms is performed for each station pair, and then the CC waveforms are stacked for desired numbers of days to obtain the CC trace S(t) of the signal. The CCs of the flag waveforms of the same pair are also computed and stacked to obtain the CC trace $F(t)$ of the flag, which represents the total number of effective points (or effective stacking times of the non-zero data) at any given time t of the CC. Next, the signal trace is normalized by the flag CC trace to obtain the final GF amplitude trace point-by-point: $A(t) = S(t)/F(t)$, which represents the true relative amplitude of the GF at time t. The computation of the flag CCs is done in the same way as the signal CCs using fast Fourier transform, thus it is simple and very efficient.

(6) The amplitudes of the GFs in the positive and negative lags of CC waveforms are generated by noise sources in opposite directions, so the causal and acausal amplitudes are extracted separately. This is in contrast of traveltime studies, where causal and acausal parts of the CC are often summed together to increase the SNR in the symmetric component of the GF (Bensen *et al.* 2007). Station pairs are sorted into a series of groups according to the azimuthal difference between pairs. In each group, the Rayleigh wave amplitude ratio between two station-pairs that originate in the same station (the amplitude from 1 to 3 divided by the amplitude from 1 to 2) is calculated, which represents the relative amplitude between the later two stations (3 relative to 2) (eq. 2). Station pairs with SNRs lower than the defined value are discarded. We measure the peak

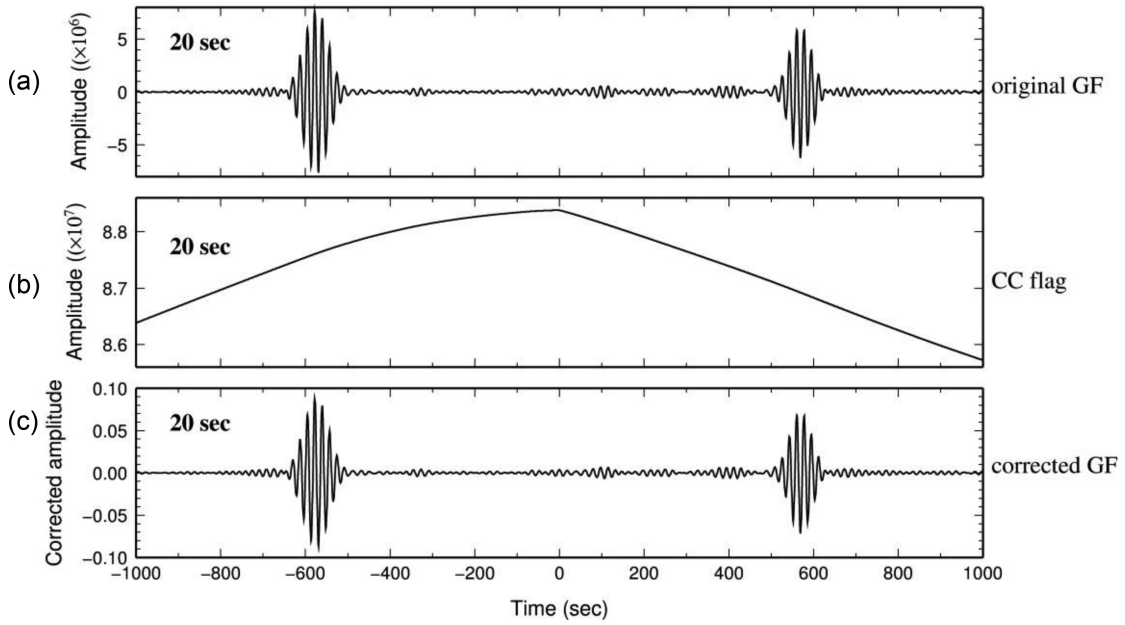

Figure 9. A generic example showing amplitude correction of GFs obtained from the ATF pre-processing. (a) The original GF from CC of continuous data of a station pair after earthquake muting and ATF pre-processing. (b) The CC of the flag traces of the same station pair as (a). (c) The corrected GF. The trace was obtained by dividing the original GF (a) by the flag trace (b) at the same delay time.

amplitude of GFs in the velocity window from 2.5 to 4.0 km s^{-1} at the periods of 10 and 20 s as the maximum amplitude of Rayleigh waves, and then we use a 200-s time window around the peak as the signal window and calculate the RMS amplitude of Rayleigh waves. We also measure the RMS amplitude of the noise in a 200-s time window starting from the end of the signal window. The ratio of the RMS amplitude of the signal to the noise is used as the SNR. Finally, we obtain the average attenuation coefficient at the assigned period by fitting the Rayleigh wave amplitude ratios satisfying the SNR criterion.

4.3 Results from real seismic data

4.3.1 Comparison between different pre-processing procedures

We now examine the effects of different pre-processing procedures with real data. For these tests, we use four U.S. Reference Network stations (US.BOZ, CI.PASC, IU.RSSD and TA.KSCO) (Fig. 1) as a network of stations for data processing.

We first compare the ATF and STF normalization methods (Fig. 10). As discussed, the STF is too restrictive, resulting in small amounts of usable data in many practical cases. The ATF is much more flexible, but doesn't include all the stations in the normalization at any given time window. With long continuous recording history with little data gaps at the RN stations, we examine whether the ATF is adequate in recovering the amplitude information. Fig. 10 compares the 20-s-period GFs of the two station pairs US.BOZ_IU.RSSD and IU.RSSD_CI.PASC obtained using the ATF and STF pre-processing procedures. After 4 yr of stacks, the difference between the relative amplitudes of the two pairs is less than 5 per cent.

We also compare the ATF with the one-bit normalization using real data (Fig. 11). The traveltimes obtained from the ATF procedure coincide with those obtained from the one-bit procedure, demonstrating that the ATF pre-processing procedure does not change the

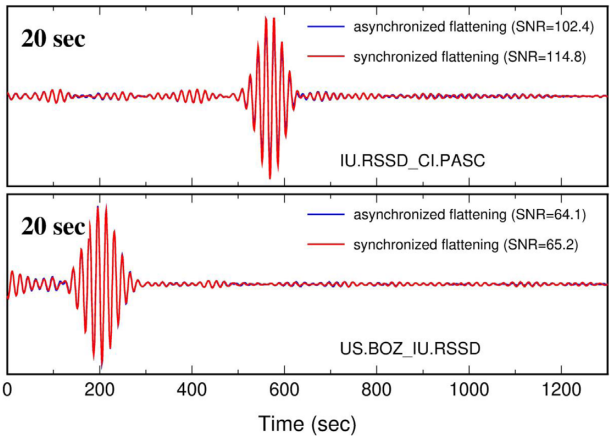

Figure 10. Comparison of GFs obtained from real data after synchronous (red) and asynchronous (blue) TF processing. Shown are two station pairs (labeled) at the period of 20 s. The two stations have long continuous recording history with few data gaps.

traveltimes of the Rayleigh waves. The SNR from the ATF is just as good as the one-bit normalization, proving that the ATF is similarly effective in the convergence of the GFs. What is more important is that the two procedures result in inconsistent relative amplitudes of GFs of the station pairs. We conclude that it is problematic to use nonlinear pre-processing on amplitudes of individual traces, such as the one-bit method, to extract amplitudes from ambient noise.

The length of the time window used in the ATF processing procedure is an important parameter in the extraction of Rayleigh wave amplitudes from ambient noise. Because the strength of noise sources may vary significantly over time, the RMS amplitude of ambient noise in too long a time window could be a poor measure of the true strength of noise in the window. We tested three time windows: 2, 6 and 24 hr (Fig. 12). The results show little difference (less than 3 per cent at the period of 20 s), and thus the AFT method

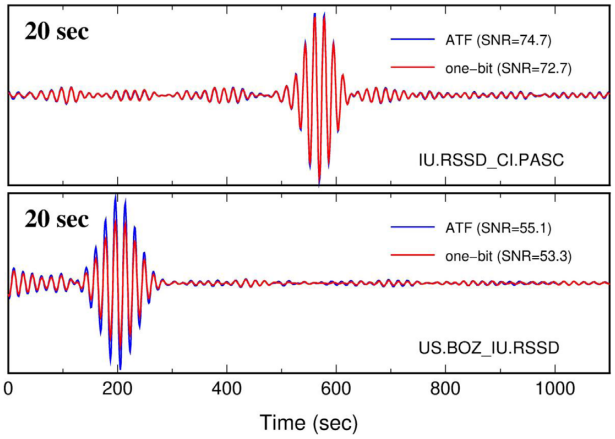

Figure 11. Comparison of GFs obtained from real data after one-bit (red) and ATF (blue) pre-processing. Shown are two station pairs (labeled) at the period of 20 s.

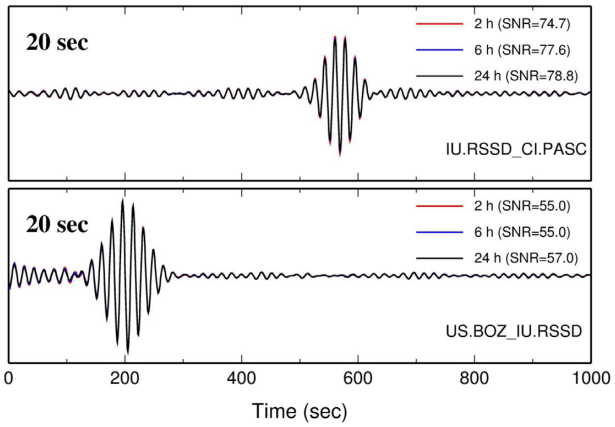

Figure 12. Tests on the length of the time window used in temporal flattening. The GFs are obtained from CCs of real data (labeled) after the ATF pre-processing. Time windows used for the temporal flattening are 2 hr (red), 6 hr (blue) and 24 hr (black), respectively. The overlapping traces are indistinguishable.

is quite tolerant. Consequently, we suggest that a 1-d time window is a good choice to perform the ATF normalization.

As mentioned above, a narrow band filtering centred on the defined period is performed on the raw data before temporal normalization and CC. Therefore, when GFs of multiple periods are calculated the entire processing procedure needs to be performed repeatedly at each period. The reason for this processing is that the strength of ambient noise often varies with periods. Compared to the traditional traveltime extraction, this procedure requires much more computing time and disk storage. Thus we tested the effects of the order of filtering (Fig. 13), applied before and after CC processing, respectively. The results show not only that the SNRs of the GFs obtained from the procedure of filtering after CC processing are much lower than those obtained from the procedure of filtering before CC processing, but also that the relative amplitudes of the GFs of the two station pairs are inconsistent. In consequence, we conclude that the filtering procedure should be performed at each trace of continuous data at each period, individually, before temporal normalization and CC processing, to obtain correct amplitude information. Such a frequency-by-frequency pre-processing before CC processing has been used by Shen *et al.* (2012), which

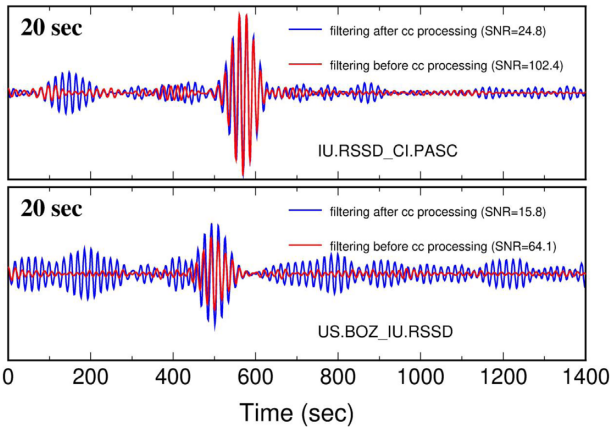

Figure 13. Tests on the order of filtering. Shown are GFs at the period of 20 s from CCs of real data (labelled) where a narrow-band-pass filter is applied before (red) and after (blue) the CC processing.

increases SNR of GFs and improves the effective data-recording duration.

4.3.2 Convergence and stability

Extending stacking days will improve the SNR of the GF of a station pair. The convergence rate is roughly proportional to the square root of the total duration (Larose *et al.* 2007; Stehly *et al.* 2008; Weaver 2011). On the one hand, increasing stacking days requires multiple folds of computing time and disk space. On the other hand, insufficient stacking days may yield unstable traveltimes or amplitudes, which will lead to incorrect attenuation solutions. The stability of traveltime measurements from ambient noise correlation has been examined previously. Bensen *et al.* (2007) show that the uncertainty of traveltimes of GFs between 3-month stacks and 12-month stacks is not obvious from the period of 5 s to the period of 100 s. In other words, the traveltime of the GF is basically stable and convergent over 3-months stacking. Zheng *et al.* (2013) also indicate that 12-month stack is sufficient to extract stable traveltimes from ambient noise.

To examine the convergence of amplitudes of GFs with stacking days, we selected 47 stations of the U.S. Reference Network (Fig. 6) to perform CCs of all station pairs by continuously increasing stacking days. We used 4 yr of continuous waveforms to investigate the convergence of GF amplitudes. Most of the stations have uninterrupted recordings, so the longest duration of continuous recordings without data gaps is about 4 yr. After muting earthquakes and spikes in the recordings and then performing CCs of station pairs, we obtained stacking CCs with the longest effective duration time of about 2 yr.

If the amplitudes of GFs with the longest effective stacking time are assumed to be stable, the ratios of the amplitudes with shorter effective stacking time to those with the longest effective stacking time can be considered as a measure of convergence (Figs 14a and b). We see that the Rayleigh wave amplitude ratios indeed become more stable as the effective stacking time increases with decreasing standard deviations. According to the variation of amplitude ratios at the periods of 10 and 20 s with stacking time (Figs 14a and b), 68 per cent Rayleigh wave amplitude ratios fluctuate less than 20 per cent when the effective stacking time reaches half a year, and the fluctuation is less than 10 per cent when the effective stacking time reaches a year.

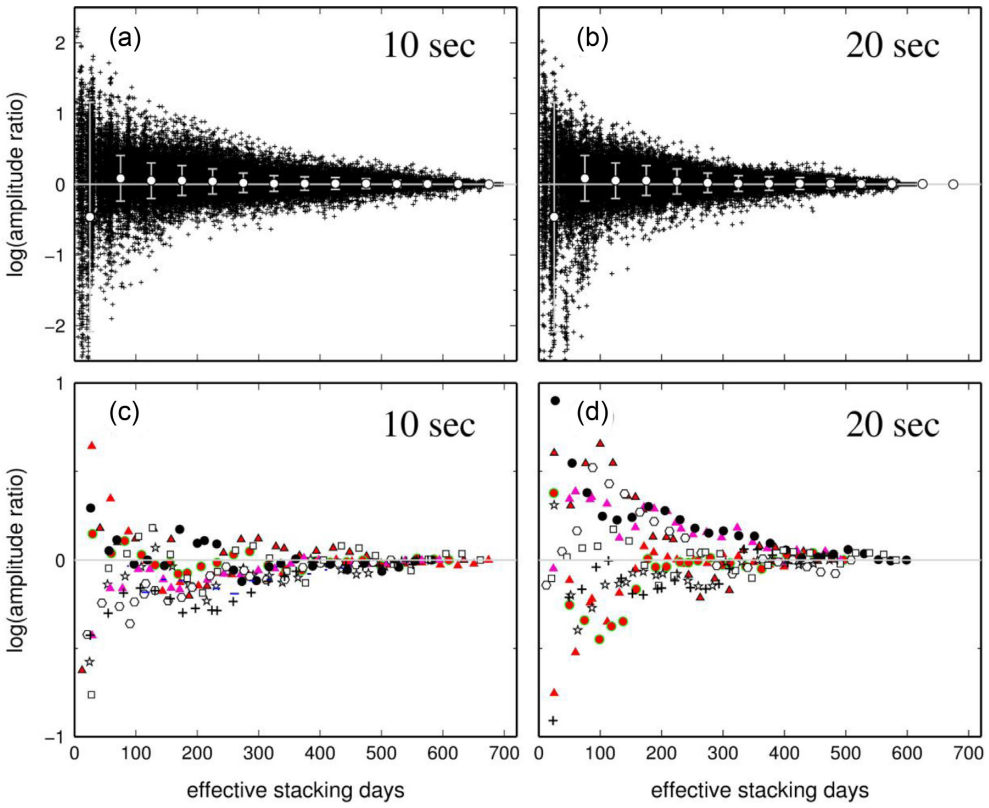

Figure 14. Examination of amplitude convergence rate with real data. For each station pair, the amplitude of the GF with longest effective stacking time is used to calibrate the convergence, that is the amplitude of the GF with a given effective stacking time is divided by that of the GF with longest effective stacking time to form an Rayleigh wave amplitude ratio. Results were obtained for all the pairs of the 47 stations in the western U.S. (Fig. 6) and for the periods of 10 and 20 s, respectively. (a, b) The logarithm of the Rayleigh wave amplitude ratios (pluses) versus stacking days. The white dots with the bars show the mean ± one standard deviation. (c, d) The logarithm of Rayleigh wave amplitude ratios versus stacking days for 10 individual station pairs (symbols).

Results of some individual pairs are also shown (Figs 14c and d). The results show that the ratios vary sharply for stacking days of less than half a year, becoming more stable as the effective stacking time increases. The average Rayleigh wave amplitude ratios and uncertainties indicate that a 0.5 to 1-yr effective stacking time is acceptable to study amplitudes of GFs from ambient noise. Roughly 2-yr of continuous overlapping data for each station are needed to generate effective 1-yr stacks. In an area of less (more) seismicity (than the Southern California), where less (more) data are muted, the ratio of the effective stacking time relative to the recording time may increase (decrease). Consequently, we suggest that, for a network of stations, more than two-years of continuous overlapping data are preferred to retrieve convergent amplitudes.

4.3.3 Attenuation from real data

To demonstrate the feasibility of the retrieval of attenuation from ambient noise, we compare results from ambient noise and those from earthquakes. We found two nearly linear arrays in western U.S. that are in similar azimuths from two earthquakes, respectively (Fig. 6). There are 121 stations in the West Line and 115 stations in the East Line. The operation time of the stations within each of the array is about 1.5 to 2 yr. Attenuation coefficients were extracted using earthquake data and ambient noise data for both arrays at periods of 10 and 20 s, respectively (Fig. 15).

For earthquake data, the traditional two-station method (e.g. Knopoff 1964; Yang *et al.* 2004; Yao *et al.* 2006) was used. Using the West Line, for example, we selected a station (NE80) close to the magnitude 5.8 earthquake in the Gulf of California as the reference station. We then constructed a linear array of stations from the USArray so that all the stations are within 5° of the great circle path of the earthquake and the reference station. We corrected the amplitude of the Rayleigh wave at each station by geometrical spreading from the earthquake (square root of distance) and then divided it by the geometrical-spreading corrected amplitude at the reference station. The average attenuation coefficient is obtained by a linear regression of the Rayleigh wave amplitude ratios. Note that we ignore site factors, which contribute to the scatter of the data. We used a similar procedure to measure the attenuation coefficients for the East Line, which includes a magnitude 6.3 earthquake and a reference station (125A). The values are 2.82 ± 0.39 ($\times 10^{-4}$ km^{-1}) at 10 s and 1.68 ± 0.69 ($\times 10^{-4}$ km^{-1}) at 20 s for the West Line and 3.95 ± 0.51($\times 10^{-4}$ km^{-1}) at 10 s and 2.59 ± 0.41 ($\times 10^{-4}$ km^{-1}) at 20 s for the East Line (Fig. 15).

For ambient noise data, we retrieve the amplitudes of the GFs of the pairs originating in the same reference station, NE80 for the West Line or 125A for the East Line (Fig. 6). The amplitudes are corrected by geometrical spreading (square root of inter-station distance) and the Rayleigh wave amplitude ratios of two station pairs are calculated using the amplitudes of the pair at larger distance by that of the pair at smaller distance. Like the earthquake data, the average attenuation coefficient is obtained by a linear regression of

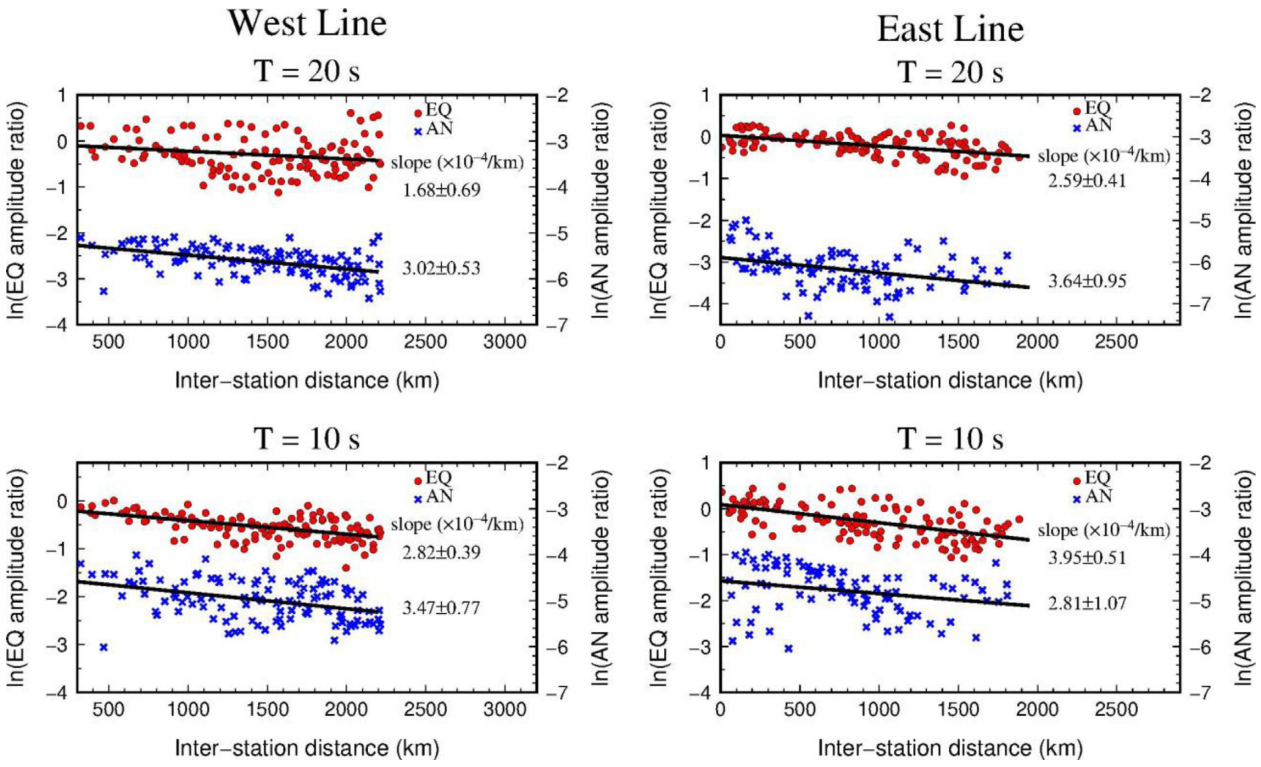

Figure 15. Attenuation retrievals for the two linear arrays (Fig. 6) using both earthquake (EQ, red dots) and ambient noise (AN, blue crosses) data at periods of 10 and 20 s. Amplitudes have been corrected by geometrical spreading. Plotted are logarithm of appropriate Rayleigh wave amplitude ratios (see text). The attenuation coefficients (labeled) are obtained from the linear regressions (black lines).

the Rayleigh wave amplitude ratios, also ignoring the influence of site factors. The values are 3.47 ± 0.77 ($\times 10^{-4}$ km^{-1}) at 10 s and 3.02 ± 0.53 ($\times 10^{-4}$ km^{-1}) at 20 s for the West Line and 2.81 ± 1.07 ($\times 10^{-4}$ km^{-1}) at 10 s and 3.64 ± 0.95($\times 10^{-4}$ km^{-1}) at 20 s for the East Line (Fig. 15).

It is worth noting that the amplitude ratios fluctuate clearly with distance and that the best fitting attenuation coefficient obtained from ambient noise is not the same as that from earthquakes. One factor for the coefficient disparity is that amplitude of seimic waves is generally hard to measure accurately. Moreover, the stations are located at the surface, and the earthquake has a certain depth, so there is a certain difference in the sampling depth of the station-pairs paths from ambient noise and earthquakes, which causes a certain difference in the fitting of average attenuation. Furthermore, the stations we used are not accurately arranged on a great circle path, but they are approximately considered to be in a same great circle path according to similar azimuths, which will also lead to the deviation of the fitting attenuation coefficients obtained from ambient noise and earthquakes. The amplitude fluctuation of different station pairs is related to the lateral inhomogeneity of attenuation, because the actual earth medium is not a uniform medium, and the attenuation varies in different regions and depths. We only fitted the average attenuation model without inversion of the lateral inhomogeneity of attenuation. The difference of site responses of different stations is also one of the reasons for the fluctuation of amplitude measurements. Although there are some differences in the attenuation coefficients obtained by earthquake and ambient noise, their magnitude is the same, and the variation trend is also very similar, so it can be considered that the values from earthquakes and ambient noise are consistent with each other within one standard deviation, except for the West Line at 20 s, where the values are within two standard deviations. These values are also generally consistent with the magnitude of attenuation obtained from earthquake-based Rayleigh-wave attenuation tomography for the western US continent (Yang *et al.* 2008a).

5 CONCLUSIONS

Following the basic theoretical derivation by Weaver (2011), we developed methods and strategies for extracting amplitude and attenuation information from ambient noise correlation. These methods were developed based on a linear array, but they can be extended to a 2-D network of stations by forming a series of linear arrays, much like the two-station method for earthquake data. Results from synthetic data reveal that the attenuation of Rayleigh waves from ambient noise CC can be retrieved correctly with TF normalization or without any temporal normalization at all. The difference is that the TF pre-processing greatly speeds up the convergence and improves the SNR of GFs. However, one-bit pre-processing, although accelerating the convergence of GFs, is not appropriate for the retrieval of attenuation. Therefore, we strongly suggest that any temporal normalization that is applied to individual traces separately should be avoided when extracting amplitude information from ambient noise.

For the real data, we suggest a detailed data processing procedure for amplitude retrieval (Fig. 7). The main steps are as follows: (1) single-station data preparation, (2) instrument response removal, (3) narrow band filtering, (4) earthquake muting and flag setting, (5) ATF, (6) CC of signal and CC of flag, (7) amplitude correction of CC and stacking and (8) measurement of amplitudes. The order of the processing steps is important and cannot be mixed. Two key

steps are narrow band filtering and the ATF normalization before CC processing.

To improve the TF normalization in practical applications, we show an improved TF method called ATF instead of the traditional STF. The ATF avoids the strict requirement on the integrity of the continuous data in the STF and does not change relative amplitudes of the GFs obtained from CCs. The GF amplitudes are not sensitive to the window length of the ATF if it is less than one day. We also find that the applying of narrow band filtering before CC processing is critical in preserving GF amplitudes; although computation cost is much lower if the narrow band filtering is performed after CC processing, the retrieved amplitudes are not correct.

The convergence of GF amplitudes with the effective stacking time indicates that longer stacking duration increases the stability of the amplitudes. We suggest that continuous data of overlapping time of 2 yr at a network of stations are preferred for the accurate retrieval of attenuation.

From our limited tests along two groups of approximately linear arrays of stations, we conclude that the attenuation coefficients are generally compatible between those obtained from ambient noise and those from two earthquakes (at periods of 10 and 20 s), respectively. Thus, our methodology of amplitude extraction appears promising in retrieving attenuation of Rayleigh waves from the ambient noise of the real Earth. The method is flexible and can be applied to linear arrays or 2-D networks of stations. Nevertheless, we didn't consider the influence of wave propagation effects in complex earth media (focusing and defocusing and site response, e.g. Bowden *et al.* 2017) on the surface wave amplitudes. Thus, in real Earth, the retrieved amplitudes from noise correlations would include contributions from attenuation and propagation, the latter of which can be evaluated from independent velocity models (Dalton & Ekström 2006). Based on the method of this study, we may further monitor the temporal changes of attenuation parameters in the underground media of the earth using ambient noise which was extensively studied by temporal change of the velocity to detect the possible earthquake precursors or coseismic velocity variations, or determine the fluid status in the underground (e.g. Brenguier *et al.* 2008a; Brenguier *et al.* 2008b; Xu & Song 2009; Chen *et al.* 2010; Cheng *et al.* 2010; Minato *et al.* 2012).

ACKNOWLEDGEMENTS

We thank Xiaoning (David) Yang for advice on extracting earthquake amplitudes by the two-station method. We thank two anonymous reviewers for constructive and insightful reviews. All of the earthquake data used in this study are available via the Incorporated Research Institutions for Seismology (IRIS) at http://www.iris.edu/hq. Most of the figures were produced with the GMT software (Wessel & Smith 1995). This study was supported by funded supported by National Natural Science Foundation of China (41774054, 41774056) and the Department of Geology, University of Illinois at Urbana-Champaign, USA.

REFERENCES

Adam, L., Batzle, M., Lewallen, K.T. & van Wijk, K., 2009. Seismic wave attenuation in carbonates, *J. geophys. Res.,* **114**(B6), B06208.

Bensen, G.D., Ritzwoller, M.H., Barmin, M.P., Levshin, A.L., Lin, F., Moschetti, M.P., Shapiro, N.M. & Yang, Y., 2007. Processing seismic ambient noise data to obtain reliable broad-band surface wave dispersion measurements, *Geophys. J. Int.,* **169**(3), 1239–1260.

Bensen, G.D., Ritzwoller, M.H. & Shapiro, N.M., 2008. Broadband ambient noise surface wave tomography across the United States, *J. geophys. Res.,* **113**(B5), B05306.

Bowden, D.C., Tsai, V.C. & Lin, F.C., 2015. Site amplification, attenuation, and scattering from noise correlation amplitudes across a dense array in Long Beach, CA, *Geophys. Res. Lett.,* **42**(5), 1360–1367.

Bowden, DC., Tsai, V.C. & Lin, F.-C., 2017. Amplification and attenuation across USArray using ambient noise wavefront tracking: USArray noise amplitudes, *J. geophys. Res.,* **122**(12), 10,086–010,101.

Brenguier, F., Shapiro, N.M., Campillo, M., Nercessian, A. & Ferrazzini, V., 2007. 3-D surface wave tomography of the Piton de la Fournaise volcano using seismic noise correlations, *Geophys. Res. Lett.,* **34**(2), 2305–2309.

Brenguier, F., Campillo, M., Hadziioannou, C., Shapiro, N.M., Nadeau, R.M. & Larose, E., 2008a. Postseismic relaxation along the San Andreas fault at Parkfield from continuous seismological observations, *Science,* **321,** 1478–1482.

Brenguier, F., Shapiro, N.M., Campillo, M., Ferrazzini, V., Duputel, Z., Coutant, O. & Nercessian, A., 2008b. Towards forecasting volcanic eruptions using seismic noise, *Nat Geosci,* **1,** 126–130.

Campillo, M. & Paul, A., 2003. Long-range correlations in the diffuse seismic coda, *Science,* **299**(5606), 547–549.

Chen, J.H., Froment, B., Liu, Q.Y. & Campillo, M., 2010. Distribution of seismic wave speed changes associated with the 12 May 2008 Mw 7.9 Wenchuan earthquake, *Geophys Res Lett,* **37,** L18302–L18305.

Cheng, X., Niu, F. & Wang, B., 2010. Coseismic velocity change in the rupture zone of the 2008 M-w 7.9 wenchuan earthquake observed from ambient seismic noise, *Bull. seism. Soc. Am.,* **100,** 2539–2550.

Cupillard, P. & Capdeville, Y., 2010. On the amplitude of surface waves obtained by noise correlation and the capability to recover the attenuation: a numerical approach, *Geophys. J. Int.,* **181**(3), 1687–1700.

Cupillard, P., Stehly, L. & Romanowicz, B., 2011. The one-bit noise correlation: a theory based on the concepts of coherent and incoherent noise, *Geophys. J. Int.,* **184**(3), 1397–1414.

Dalton, C.A. & Ekström, G., 2006. Global models of surface wave attenuation, *J. geophys. Res.,* **111,** B50317. doi:10.1029/2005JB003997.

Froment, B., Campillo, M., Roux, P., Gouedard, P., Verdel, A. & Weaver, R.L., 2010. Estimation of the effect of nonisotropically distributed energy on the apparent arrival time in correlations, *Geophysics,* **75**(5), SA85.

Gerstoft, P. & Tanimoto, T., 2007. A year of microseisms in southern California, *Geophys. Res. Lett,* **34**(20), L20304.

Groos, J.C., Bussat, S. & Ritter, J.R.R., 2011. Performance of different processing schemes in seismic noise cross-correlations, *Geophys. J. Int.,* **188**(2), 498–512.

Johnston, D.H., Toksöz, M.N. & Timur, A., 1979. Attenuation of seismic waves in dry and saturated rocks: II. Mechanisms, *Geophysics,* **44**(4), 691–711.

Kang, T.S. & Shin, J.S., 2006. Surface-wave tomography from ambient seismic noise of accelerograph networks in southern Korea, *Geophys. Res. Lett.,* **33**(17), L17303.

Karato, S-i., 1993. Importance of anelasticity in the interpretation of seismic tomography, *Geophys. Res. Lett.,* **20**(15), 1623–1626.

Karato, S-i., 2003. Mapping water content in upper mantle, *Geophys. Mono.,* **138**(1), 135–152.

Knopoff, L., 1964. Q, *Rev. Geophys.,* **2**(4), 625–660.

Kohler, M.D., Heaton, T.H. & Bradford, S.C., 2007. Propagating waves in the steel, moment-frame factor building recorded during earthquakes, *Bull. seism. Soc. Am.,* **97**(4), 1334–1345.

Komatitsch, D., Liu, Q., Tromp, J., Süss, P., Stidham, C. & Shaw, J.H., 2004. Simulations of ground motion in the Los Angeles basin based upon the spectral-element method, *Bull. seism. Soc. Am.,* **94**(1), 187–206.

Larose, E., Roux, P. & Campillo, M., 2007. Reconstruction of Rayleigh-Lamb dispersion spectrum based on noise obtained from an air-jet forcing, *J. acoust. Soc. Am.,* **122**(6), 3437–3444.

Lawrence, J.F. & Prieto, G.A., 2011. Attenuation tomography of the western United States from ambient seismic noise, *J. geophys. Res.,* **116**(B6), B06302–B06312.

Lawrence, J.F., Denolle, M., Seats, K.J. & Prieto, G.A., 2013. A numeric evaluation of attenuation from ambient noise correlation functions, *J. geophys. Res.* **118**(12), 6134–6145.

Lin, F.-C., Moschetti, M.P. & Ritzwoller, M.H., 2008. Surface wave tomography of the western United States from ambient seismic noise: Rayleigh and Love wave phase velocity maps, *Geophys. J. Int.,* **173**(1), 281–298.

Lin, F.-C., Ritzwoller, M.H. & Shen, W., 2011. On the reliability of attenuation measurements from ambient noise cross-correlations, *Geophys. Res. Lett.,* **38**(11), L11303–L11308.

Liu, X., Ben-Zion, Y. & Zigone, D., 2015. Extracting seismic attenuation coefficients from cross-correlations of ambient noise at linear triplets of stations, *Geophys. J. Int.,* **203**(2), 1149–1163.

Lobkis, O.I. & Weaver, R.L., 2001. On the emergence of the Green's function in the correlations of a diffuse field, *J. acoust. Soc. Am.,* **110**(6), 3011–3017.

Matzel, E., 2007. Imaging seismic attenuation in the crust and upper mantle by ambient noise correlation, *EOS, Trans. Am. Geophys. Un.,* **88**(52), Fall Meet. Suppl., Abstract S33E-08.

Matzel, E.M., 2008. Attenuation tomography using ambient noise correlation, *EOS, Trans. Am. Geophys. Un.,* **89**(53), Abstract S24A–04.

Minato, S., Tsuji, T., Ohmi, S. & Matsuoka, T., 2012. Monitoring seismic velocity change caused by the 2011 Tohoku-oki earthquake using ambient noise records, *Geophys. Res. Lett.,* **39**. doi:10.1029/2012GL051405.

Mordret, A., Sun, H., Prieto, G.A., Toksöz, M.N. & Büyüköztürk, O., 2017. Continuous monitoring of high-rise buildings using seismic interferometry, *Bull. seism. Soc. Am.,* **107**(6), 2759–2773.

Nakahara, H., 2006. A systematic study of theoretical relations between spatial correlation and Green's function in one-, two- and three-dimensional random scalar wavefields, *Geophys. J. Int.,* **167**(3), 1097–1105.

Nakata, N. & Snieder, R., 2014. Monitoring a building using deconvolution interferometry. II: ambient-vibration analysis, *Bull. seism. Soc. Am.,* **104**(1), 204–213.

Nakata, N., Snieder, R., Kuroda, S., Ito, S., Aizawa, T. & Kunimi, T., 2013. Monitoring a building using deconvolution interferometry. I: earthquake-data analysis, *Bull. seism. Soc. Am.,* **103**(3), 1662–1678.

Olsen, K. *et al.*, 2006. Strong shaking in Los Angeles expected from southern San Andreas earthquake, *Geophys. Res. Lett.,* **33**(7), 1–4.

Priestley, K. & McKenzie, D., 2006. The thermal structure of the lithosphere from shear wave velocities, *Earth planet. Sci. Lett.,* **244**(1), 285–301.

Prieto, G.A. & Beroza, G.C., 2008. Earthquake ground motion prediction using the ambient seismic field, *Geophys. Res. Lett,* **35**(14), L14304–14308.

Prieto, G.A., Lawrence, J.F. & Beroza, G.C., 2009. Anelastic Earth structure from the coherency of the ambient seismic field, *J. geophys. Res.,* **114**(B7), B07303.

Prieto, G.A., Lawrence, J.F., Chung, A.I. & Kohler, M.D., 2010. Impulse response of civil structures from ambient noise analysis, *Bull. seism. Soc. Am.,* **100**(5A), 2322–2328.

Prieto, GA., Denolle, M., Lawrence, J.F. & Beroza, G.C., 2011. On amplitude information carried by the ambient seismic field, *C.R. Geosci.,* **343**(8–9), 600–614.

Sabra, K.G., Gerstoft, P., Roux, P., Kuperman, W.A. & Fehler, M.C., 2005. Surface wave tomography from microseisms in Southern California, *Geophys. Res. Lett.,* **32**(14), L14311–L14314.

Shapiro, N.M. & Campillo, M., 2004. Emergence of broadband Rayleigh waves from correlations of the ambient seismic noise, *Geophys. Res. Lett,* **31**(7), 1615–1619.

Shapiro, N.M., Campillo, M., Stehly, L. & Ritzwoller, M.H., 2005. High-resolution surface-wave tomography from ambient seismic noise, *Science,* **307**(5715), 1615–1618.

Shen, Y., Ren, Y., Gao, H. & Savage, B., 2012. An improved method to extract very-broadband empirical green's functions from ambient seismic noise, *Bull. seism. Soc. Am.,* **102**(4), 1872–1877.

Snieder, R. & Safak, E., 2006. Extracting the building response using seismic interferometry: theory and application to the Millikan Library in Pasadena, California, *Bull. seism. Soc. Am.,* **96**(2), 586–597.

Stehly, L., Campillo, M. & Shapiro, N.M., 2006. A study of the seismic noise from its long-range correlation properties, *J. geophys. Res.,* **111**(B10), B10306.

Stehly, L., Campillo, M., Froment, B. & Weaver, R.L., 2008. Reconstructing Green's function by correlation of the coda of the correlation (C3) of ambient seismic noise, *J. geophys. Res.,* **113**(B11), B11306.

Stehly, L. & Boué, P., 2017. On the interpretation of the amplitude decay of noise correlations computed along a line of receivers, *Geophys. J. Int.,* **209** (1), 358–372.

Sun, H., Mordret, A., Prieto, G.A., Toksöz, M.N. & Büyüköztürk, O., 2017. Bayesian characterization of buildings using seismic interferometry on ambient vibrations, *Mech. Syst. Signal. Pr.,* **85,** 468–486.

Sun, X., Song, X., Zheng, S., Yang, Y. & Ritzwoller, M.H., 2010. Three dimensional shear wave velocity structure of the crust and upper mantle beneath China from ambient noise surface wave tomography, *Earthq. Sci.,* **23**(5), 449–463.

Taylor, S.R., Gerstoft, P. & Fehler, M.C., 2009. Estimating site amplification factors from ambient noise, *Geophys. Res. Lett,* **36**(9), L09303.

Toksöz, M.N., 1979. Attenuation of seismic waves in dry and saturated rocks: I. Laboratory measurements, *Geophysics,* **44**(4), 681–690.

Tsai, V.C., 2011. Understanding the amplitudes of noise correlation measurements, *J. geophys. Res.,* **116**(B9), B09311.

Viens, L., Denolle, M., Miyake, H., Sakai, S. & Nakagawa, S., 2017. Retrieving impulse response function amplitudes from the ambient seismic field, *Geophys. J. Int.,* **210**(1), 210–222.

Weaver, R.L., 1982. On diffuse waves in solid media, *J. acoust. Soc. Am.,* **71,** 1608–1609.

Weaver, R.L., 2001. Equipartition and mean-square responses in large undamped structures, *J. acoust. Soc. Amer.,* **110**(2), 894–903.

Weaver, RL., 2011. On the amplitudes of correlations and the inference of attenuations, specific intensities and site factors from ambient noise, *C.R. Geosci.,* **343**(2011), 615–622.

Weaver, RL., 2013. On the retrieval of attenuation and site amplifications from ambient noise on linear arrays: further numerical simulations, *Geophys. J. Int.,* **193**(3), 1644–1657.

Wessel, P. & Smith, W.H.F., 1995. New version of the generic mapping tools, *EOS, Trans. Am. Geophys. Un.,* **76,** 329–329.

Winkler, K. & Nur, A., 1979a. Friction and seismic attenuation in rocks, *Nature,* **277**(1979), 528–531.

Winkler, K. & Nur, A., 1979b. Pore fluids and seismic attenuation in rocks, *Geophys. Res. Lett.,* **6**(1), 1–4.

Winkler, K.W. & Nur, A., 1982. Seismic attenuation: effects of pore fluids and frictional sliding, *Geophysics,* **47**(1), 1–15.

Xu, Z.J. & Song, X., 2009. Temporal changes of surface wave velocity associated with major Sumatra earthquakes from ambient noise correlation, *Proc. Natl. Acad. Sci.,* **106,** 14207–14212.

Yang, X., Taylor, S.R. & Patton, H.J., 2004. The 20-s Rayleigh wave attenuation tomography for central and southeastern Asia, *J. geophys. Res.,* **109**(B12), B12304–B12304.

Yang, Y. & Forsyth, D.W., 2008a. Attenuation in the upper mantle beneath Southern California: physical state of the lithosphere and asthenosphere, *J. geophys. Res.,* **113**(B3), B03308–B03308.

Yang, Y., Ritzwoller, M.H., Lin, F.C., Moschetti, M.P. & Shapiro, N.M., 2008b. Structure of the crust and uppermost mantle beneath the western United States revealed by ambient noise and earthquake tomography, *J. geophys. Res.,* **113**(B12), B12310–B12310.

Yao, H. & Van Der Hilst, R.D., 2009. Analysis of ambient noise energy distribution and phase velocity bias in ambient noise tomography, with application to SE Tibet, *Geophys. J. Int.,* **179**(2), 1113–1132.

Yao, H., Van Der Hilst, R.D. & De Hoop, M.V., 2006. Surface-wave array tomography in SE Tibet from ambient seismic noise and two-station analysis–I. Phase velocity maps, *Geophys. J. Int.,* **166**(2), 732–744.

Zhang, J. & Yang, X., 2013. Extracting surface wave attenuation from seismic noise using correlation of the coda of correlation, *J. geophys. Res.,* **118**(5), 2191–2205.

Zheng, S., Sun, X., Song, X., Yang, Y. & Ritzwoller, M.H., 2008. Surface wave tomography of China from ambient seismic noise correlation, *Geochem. Geophys. Geosyst.,* **9**(5), Q05020.

Zheng, X., Zhao, C., Zhou, L. & Zheng, S., 2013. Reliability analysis of retrieving surface waves from ambient noise data between seismic station Pairs: an example of application at broadband stations in centeral and eastern China, *Acta Seism. Sin.,* **35**(2), 218–228.

Zhou, L., Zhao, C., Chen, Z. & Zheng, S., 2011a. Amplitude tomography of Lg waves in Xinjiang and its adjacent regions, *Bull. seism. Soc. Am.,* **101**(3), 1302–1314.

Zhou, L., Zhao, C., Zheng, X., Chen, Z. & Zheng, S., 2011b. Inferring water infiltration in the Longtan reservoir area by three-dimensional attenuation tomography: 3-D Q models in the Longtan reservoir area, *Geophys. J. Int.,* **186**(3), 1045–1063.